Construction of a global gas-dynamical model for our galaxy

Mulder, W.A.; Liem, B.T.

Astron. Astrophys. 157, 148–158 (1986)

ASTRONOMY AND ASTROPHYSICS

Construction of a global gas-dynamical model for our Galaxy

W. A. Mulder[1,2] **and B. T. Liem**[1]

[1] Sterrewacht, Huygens Laboratorium, P.O. Box 9513, NL-2300 RA Leiden, The Netherlands
[2] Department of Computer Science, Stanford University, Stanford, CA 94305, USA

Received July 8, accepted September 13, 1985

Summary. This paper describes an initial effort to construct a global gas-dynamical model for our Galaxy. The model is a two-dimensional quasi-steady solution of the gas-dynamical equations in the gravitational potential of a weakly barred galaxy. From this solution we construct longitude-velocity diagrams that are compared with observations of neutral hydrogen in our Galaxy.

The main problem is the determination of the "best" position for the sun in our model. We find a position that, for the present model, correctly reproduces the 3-kpc arm, the high velocities near the centre, the "forbidden" velocities near the centre and anticentre, and some other distinct features in the observations.

It turns out that the (l, v)-diagram is mainly determined by the non-circular velocity field of our numerical solution. This implies that the interpretation of the observed (l, v)-distribution in terms of high-density arms and circular motion may lead to incorrect results.

The rotation curve corresponding to the axisymmetric part of the potential is proportional to $R^{0.1}$. The bar generates large deviations from this rotation curve. The model (l, v)-diagram has high-velocity wings near the centre. This indicates that the central peak in the observed galactic rotation curve is mainly due to highly non-circular motions. As a consequence, the interpretation of this peak in terms of circular motion is bound to overestimate the mass of the central stellar component.

Key words: structure of the Galaxy – kinematics and dynamics of the Galaxy – barred galaxy – hydrodynamics

1. Introduction

Since the early neutral hydrogen observations of the Milky Way in the 1950's, the large-scale structure of our Galaxy has been a subject of intensive study by both observers and theoreticians. "In the meantime, the question of galactic spiral structure remains, as over the past 30-year history of HI, open." The last conclusion, quoted from a review by Liszt (1985), pointedly summarizes the current state of affairs.

The main hindrance for disentangling apparent structures in the data is, of course, our own position right in the middle of the pattern. Additional problems are caused by the irregular nature of the neutral hydrogen distribution on smaller scales, a nature similar to that in other galaxies. When viewed too closely, any large-scale pattern seems to disappear, or, worse, new structures seem to show up that are not really there (Liszt and Burton, 1981). Furthermore, the representation of observed line-profiles in longitude-velocity diagrams reveals ridges and loops that are partly caused by high densities in specific regions of our Galaxy, but also, and to a significant extent, by a concentration of *velocities* along the line of sight. This *velocity crowding* is an important effect in the presence of non-circular motion and causes material at different positions, but with the same radial velocity, to appear as a ridge in the (l, v)-diagram. This considerably complicates the interpretation of these diagrams. It is difficult, if not impossible, to unambiguously determine a large-scale pattern from the observations.

On the other hand, one can hope to reconstruct a global pattern on the basis of an acceptable *physical* model. Such a model may provide the additional information required for a correct interpretation of the data. Attempts along these lines have been made on the basis of the density-wave theory, e.g., by Yuan (1969), Burton (1971), and Simonson (1976). The main drawback of the models is the freedom to construct almost any kind of spiral pattern. This leads to a sophisticated kind of curve fitting and at the same time discards any additional information that might be supplied by a proper physical model.

The obvious need is for a physical model based on as few parameters as possible. It should at least give a good explanation for those features in the observed (l, v)-diagrams that can be identified without ambiguity. One then may hope to find a correct interpretation for other patterns by looking at the model. This is the motivation for the present work.

Our model is a two-dimensional quasi-steady solution of the gas-dynamical equations in the gravitational potential of a weakly barred galaxy. The suggestion that our Galaxy contains a bar has already been made by Kerr (1967) as an explanation for the 3-kpc arm. A *kinematical* model for this arm was made by Peters (1975) on the basis of a flow pattern suggested by Roberts (1971). Only recently, two *gas-dynamical* models for the 3-kpc arm have been presented. The first one, by Yuan (1984), assumes a spiral density-wave with an extremely rapid rotation, that drives an arm at the Outer Lindblad Resonance. The gas in that arm has the desired radial velocity. The second, more plausible, model, by van Albada (1985), is based on a fully two-dimensional time-dependent computation of the gas flow in a barred galaxy, and provides an arm with a similar radial velocity under more reasonable assumptions.

Here we use a two-dimensional quasi-steady numerical solution of the Euler equations for isothermal gas flow. The potential is a simple power law with a weak bar-like perturbation, as used in two earlier papers (Mulder and Hooimeyer, 1984, Paper I;

Send offprint requests to: W. A. Mulder (American address)

Mulder, 1986, Paper II). We deliberately use this simple form rather than a more sophisticated mass model for our Galaxy, because the actual form of the latter may be affected by a wrong interpretation of measured velocities. The power of the potential can be derived from observed rotation curves of other galaxies. For that reason it is kept fixed. This leaves the axial ratio of the bar as a free parameter. In addition, we allow the bar to end either at co-rotation (CR) or at the Outer Lindblad Resonance (OLR).

The numerical method for finding the quasi-steady state is described in Paper II. It efficiently computes a steady solution of the Euler equations by means of multigrid relaxation.

In the next section we describe the potential and the method of constructing (l, v)-diagrams from our model. Section 3 describes the search for the "best" position of the Local Standard of Rest (LSR) in the model. The result and the comparison with the observations are presented in Sect. 4. Some concluding remarks are made in Sect. 5.

2. Model

Our model is a quasi-steady solution of the gas-dynamical equations in the gravitational potential of a weakly barred galaxy. The basic assumptions leading to the choice of the two-dimensional isothermal Euler equations as a description of the gaseous components of the interstellar medium are described by Shu et al. (1972). Paper II describes the numerical technique for the computation of the quasi-stationary solution.

The potential in the plane of the galaxy is a power law with a bar-like perturbation:

$$V(R,\phi)=R^{p+2}(c_0+c_2(R)\cos(2\phi)). \tag{1}$$

Here R and ϕ are galactocentric polar co-ordinates in the equatorial plane, with ϕ measured counterclockwise with respect to the positive x-axis of our model, corresponding to the long axis of the bar. For the power we choose $p=-1.8$, in accordance with observations of the galactic bulge (Sanders and Lowinger, 1972; Isaacman, 1981) and measured rotation curves of Sc galaxies (Burstein et al., 1982) and Sb galaxies (Rubin et al., 1982). Note that no distinction is made among bulge-, disk-, and halo-components in our model.

The amplitude $c_2(R)$ of the bar relative to c_0 is related to its axial ratio. If the bar extends to infinity, $c_2(R)$ is a constant. The R-dependence comes in if the bar is cut off at a certain radius. For a weak bar, the amplitude $c_2(R)$ is much smaller than c_0. Further details can be found in Papers I and II.

The thin disk of gas is assumed to be in hydrostatic equilibrium against the vertical component of the gravitational potential. The density of the gas can be written as

$$\varrho(R,\phi,z)=\varrho(R,\phi,0)\exp(-1/2\,z^2/H^2), \tag{2}$$

where the scaleheight H may depend on R and ϕ. Because H is generally much smaller than R, the full three-dimensional problem can be replaced by a set of equations in two dimensions. The solution of these equations yields a surface density ϱ_s, a radial velocity u_R, and a tangential velocity u_ϕ, as a function of R and ϕ. The rotational velocity u_ϕ is positive for clockwise rotation. This choice introduces a minus sign in the relation between u_ϕ and $\dot{\phi}$, since the latter is measured counterclockwise. Note that u_R and u_ϕ refer to the galactocentric co-ordinates in an inertial frame. The line-of-sight velocity, which is radial with respect to the LSR, will be denoted by $v_{\rm rad}$ or simply v. The surface density is related to the local density in the plane by

$$\varrho_s(R,\phi)=\int_{-\infty}^{\infty} dz\,\varrho(R,\phi,z)=\sqrt{2\pi}\,H\varrho(R,\phi,0). \tag{3}$$

For the scaleheight H we assume the following dependence on R:

$$H=H_0 \quad \text{if} \quad R\leqq R_0, \tag{4a}$$

$$H=H_0+\alpha_1(R-R_0)^2 \quad \text{if} \quad R_0<R<R_1, \tag{4b}$$

$$H=H_0+\alpha_2(R-R_0) \quad \text{if} \quad R\geqq R_1. \tag{4c}$$

The angular dependence is neglected. Within R_0 the scaleheight is assumed to be constant. A typical value for H_0 is 120 pc (Spitzer, 1978). Outside R_1 the scaleheight increases linearly with R. This assumption is based on results by Kulkarni et al. (1982), from which a value $\alpha_2=0.084$ can be derived. Equation (4b) merely provides a smooth transition from the constant to the linear part of the scaleheight. If R_0 and α_2 are specified, the requirement of smoothness implies

$$\xi=2H_0/\alpha_2, \quad \alpha_1=\alpha_2/(2\xi), \quad R_1=R_0+\xi. \tag{5}$$

A choice has to be made for R_0: we, rather arbitrarily, adopt the co-rotation radius $R_{\rm CR}$ of the model.

The observations of neutral hydrogen in our Galaxy can be displayed in the form of longitude-velocity diagrams. In order to make a comparison between our model and these observations, we have to transform the set of quantities ϱ_s, u_R, and u_ϕ as a function of the position (R,ϕ) in the model to a corresponding (l, v)-diagram. This requires a position for the LSR in our model. Once this position has been chosen, the model is automatically scaled. The problem is, of course, to find the "best" position of the LSR, given a certain model. This will be discussed in the next section.

We continue with the technical details of the construction of model (l, v)-diagrams. As mentioned above, a choice for the position of the LSR defines the scales of the model. Let r_0 be the unit of length and u_0 the unit of velocity in our model. These units are expressed in physical units by the relations

$$r_0=10\ \text{kpc}/R_{\rm LSR},\ u_0=250\ \text{km s}^{-1}/u_{\phi,\rm LSR}. \tag{6}$$

Here $R_{\rm LSR}$ is the distance of the LSR to the galactic centre and $u_{\phi,\rm LSR}$ the rotational velocity of the LSR, both expressed in model units. For the rotational velocity we use a value based on the axisymmetric part of the potential:

$$u_{\phi,\rm LSR}=((p+2)c_0)^{1/2}R_{\rm LSR}^{1+1/2p}. \tag{7}$$

The radial velocity $u_{R,\rm LSR}$ is assumed to be zero. For a given position $(R_{\rm LSR},\phi_{\rm LSR})$ in the model we want to find the distribution of the brightness temperature $T(l, v)$. In view of the assumption of constant temperature, the brightness temperature can be related to the optical depth $\tau(l, v)$ by

$$T(l,v)=T_0(1-\exp(-\tau(l,v))). \tag{8}$$

For the gas kinetic temperature T_0 we adopt 120 K. The optical depth along the line of sight, for given l and v, is found from

$$\tau(l,v)=\int_0^{s_{\max}} d\tau(l,v), \tag{9a}$$

where

$$d\tau(l,v)=\frac{1.69\,10^3}{T(K)}\frac{r_0(\text{kpc})}{u_0(\text{km/s})}n_{\rm HI}(\text{cm}^{-3})\,P(v-v_{\rm rad}(l,s))\,ds. \tag{9b}$$

Here s is the distance from the LSR, measured along the line of sight in model units. The numerical constant is computed from

values in Spitzer (1978). The temperature T equals the constant T_0 mentioned above. The unit of length r_0 provides the proper scaling for s; u_0 does the same for the velocity distribution $P(w)$. The latter is a gaussian:

$$P(w)=\frac{1}{\sigma\sqrt{2\pi}}\exp(-1/2\,w^2/\sigma^2), \tag{10}$$

where σ denotes the velocity dispersion of the gas. For our model, it is convenient to improve the resolution by choosing σ smaller than the usual value of 5 km s^{-1}. We use $\sigma=0.2\,c$. The sound speed c denotes an effective value for the mixture of gaseous components in the Interstellar Medium. Its value is taken to be 0.035 in our model units.

The local density of the gas is related to the surface density by

$$n_{\rm HI}=n_{\rm HI,0}\,\frac{\varrho_s(l,s)}{\varrho_{s,0}}\,\frac{H_0}{H(l,s)}. \tag{11}$$

Here $\varrho_{s,0}$ is a reference density for the surface density of our model: we adopt the average of ϱ_s over the area within co-rotation. The reference density $n_{\rm HI,0}$ is of the order of 1 cm^{-3}. Instead of adopting the observed value, we use $n_{\rm HI,0}$ to provide the proper scaling of the temperature in the model (l,v)-diagram. Note that Eq. (11) implies the assumption that the neutral hydrogen everywhere constitutes a constant percentage of the total amount of gas.

The actual numerical evaluation of $T(l,v)$ is done in the same way as by Burton (1971), but with some improvements. We define an array τ_{ij}, where i denotes a sequence of longitudes l_i, separated by Δl, and j a sequence v_j, spaced by Δv. For the evaluation of Eq. (9), we march along the line of sight, with increasing s. The increment Δs is allowed to vary, in order to follow details of the solution without wasting computational efforts in slowly varying regions of the flow. At every discrete s_k, the local density $n_{\rm HI}$ and radial velocity $v_{\rm rad}$ with respect to the LSR are computed. Both values are averaged with the previous ones at s_{k-1}, and the average density $n_{\rm HI}$ as given in Eq. (11), multiplied by the actual value of Δs, is added to τ_{ij}. The index j corresponds to the average radial velocity $v_{\rm rad}$ between s_{k-1} and s_k. The integration is stopped at $s_{\rm max}$, which is determined by the radius where the disk is cut off. In principle, our solution extends to infinity. At large radii, well beyond the OLR, the surface density is constant, the radial velocity u_R vanishes and the tangential velocity u_ϕ is determined by the axisymmetric part of the potential, in the same way as given in Eq. (7). In practice, the extent of the disk is limited by specifying a maximum radius. After the integration along the line of sight, the convolution with the guassian $P(w)$ of Eq. (10) is carried out. The results are multiplied by the remaining factors of Eq. (9b) and then converted to the brightness temperature.

The parameters that determine our model (l,v)-diagram are summarized below.

(i) The gravitational potential is determined by its power p and the axial ratio b/a of the short axis with respect to the long axis of the bar. For p we use -1.8. In addition, a cut-off radius for the bar is required, which is chosen either at CR or at the OLR.

(ii) Other than on the potential, the flow field of the model depends on the sound speed c. We always use $c=0.035$, where c is expressed in model unit, as in Paper II. Once the position of the LSR has been chosen, the sound speed can be expressed in physical units through Eq. (6). At the end of Sect. 3 we will find $c=10.9$ km s^{-1} for our "best" position of the LSR.

(iii) The other parameters describe the transformation from the model quantities ϱ_s, u_R, and u_ϕ to $T(l,v)$. We use the values given above, unless specified otherwise.

In short, the only basic freedom we allow ourselves, is the choice of the axial ratio of the bar and its cut-off radius. In addition, the model (l,v)-diagram is determined by the choice of the position of the LSR.

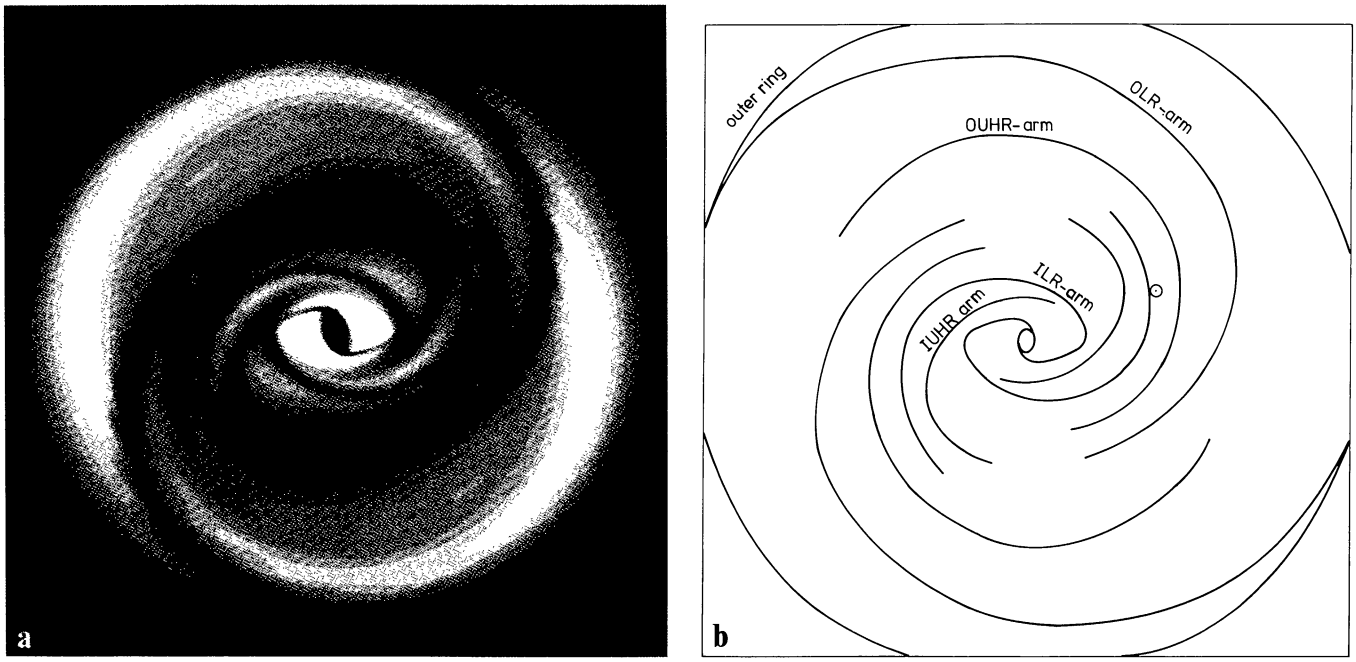

Fig. 1. a Surface density of our model for a bar with an axial ratio 0.7, ending at the OLR. A darker shade corresponds to a higher density. The sides of the figure correspond to 40 units of length. The ILR is at a radius of 1.86, the IUHR at 5.00, CR at 8.36, the OUHR at 11.87 and the OLR at 15.49. The long axis of the bar coincides with the horizontal axis. **b** Sketch of the spiral arms based on **a**. The various arms are named after the resonances

We end this section with a description of a quasi-steady solution. Figure 1a shows the surface density for a bar with an axial ratio 0.7 ending at the OLR. In the terminology of Paper II, this results in a Type II solution with shocks both inside and outside CR. The cut-off of the bar is accomplished by means of the weighting function described in Eq. (A1.6) of Paper I, using the powers $i=4$ and $j=2$. For the potential, we have a constant $c_0=2.1160$. The function $c_2(R)$ has a practically constant value of -0.028844 near the centre. The weighting function causes $|c_2|$ to decrease if R approaches the OLR. Outside the OLR, $c_2(R) = -4.1205\,10^{-3}(R/R_{\rm OLR})^{-3.2}$. The pattern speed of the bar is $\omega=0.096213$, causing CR to be at 8.3612. Further details can be found in Paper I.

As mentioned in Paper II, dissipation by shocks causes inflow inside, and outflow outside co-rotation. This conflicts with the numerical scheme, which has been designed for the efficient computation of stationary flows. A quasi-steady solution can be obtained if depletion of the region around CR is prohibited by an additional source term that adds gas in low-density regions and removes material from high-density regions. This keeps the density range within acceptable limits. Here we use a source term that is slightly different from the one in Paper II, in that the prescribed velocity of the material that is added or removed, equals the local velocity rather than zero velocity. The constant α_M of Eq. (24) in Paper II is taken to be 10^{-4}.

The introduction of the additional source term is motivated by the numerical scheme. It should not affect the physics of the solution. As shown in Paper II, the timescale corresponding with α_M is larger than the Hubble time. Therefore, the effect of depletion around co-rotation is not very significant. A different value of α_M results in a solution with a practically unaltered velocity field. Only the average density per ring, $\langle\varrho_s\rangle=1/(2\pi)\int_0^{2\pi} d\phi\varrho_s(R,\phi)$ as a function of R is affected. The quantities $\varrho_s/\langle\varrho_s\rangle$, u_R and u_ϕ are practically time-independent once the spiral pattern has been generated. Only the average density per ring $\langle\varrho_s\rangle$ varies slowly in time, and this is suppressed by the additional source term. As a consequence, the radial dependence of $\langle\varrho_s\rangle$ will be only qualitatively correct in our numerical solution. Fortunately, as will turn out in Sect. 4, the model (l,v)-diagrams are fairly independent of the density distribution in our model galaxy.

Figure 1b is a sketch corresponding to Fig. 1a. It shows the main features of the quasi-steady solution. In the centre there is a small ring, from which two arms spiral outward, across the Inner Lindblad or 1:2 resonance. The ratio indicates $(\omega_0-\omega):\omega_1$, where ω_0 is the rotation frequency, ω_1 the epicycle frequency, and ω the pattern speed of the bar. At the Inner Ultra-Harmonic or 1:4 resonance (IUHR) two extra arms appear, resulting in a four-armed spiral pattern in this region. Around CR all the arms vanish. The shocks inside CR occur on the *inside* of the spiral arms. Outside CR, the shocks are along the *outside* of the spiral arms. There are two strong arms at the Outer Lindblad or $-1:2$ resonance and again two additional arms at the Outer Ultra-Harmonic or $-1:4$ resonance (OUHR). The arms at the OLR continue outwards until they end in a ring where the shocks disappear.

3. The position of the LSR

If it is assumed that our model is more or less correct, our task is to find a position for the LSR that gives the "best" correspondence with the observed (l,v)-distribution. A number of methods that may lead to a proper choice are discussed below.

Our first approach is based on the tangential points. These lie, by definition, on a circle through the LSR and the Galactic Centre (GC). In the case of purely circular motion with a flat rotation curve, the maximum radial velocity $v_{\rm rad}$ (corrected for σ) measured along the line of sight for $|l|<90°$ is due to material at the tangential points. At this point, the rotational velocity v is parallel to the line of sight. Or, for a fixed l, the tangential point is the position on the line of sight that is nearest to the GC. Any change of the velocity at the tangential point may show up as an irregularity, or bump, in the otherwise smooth (l,v)-diagram. If it is assumed that the change in the rotational velocity is associated with a nearby spiral arm, the occurrence of bumps or peaks in the (l,v)-diagram can be related to a spiral arm near the tangential point.

This method is usually applied to find the distance of spiral arms to the LSR from the observed (l,v)-distribution. Here it is used to determine the position of the LSR in our model. Suppose we have a set of values $\{l_k\}$, with $k=1,2,\ldots$, the longitudes of suspected bumps in the observed (l,v)-distribution. The positions $(R,\phi)_k$ of the arms at those points can be related to the position of the LSR by

$$R_{\rm LSR}=R_k/\cos(l_k)\,, \tag{12a}$$

$$\phi_{\rm LSR}=\phi_k-l_k+\mathrm{sign}(l_k)\cdot 90°\,. \tag{12b}$$

Here ϕ is measured counterclockwise with respect to the long axis of the bar, the horizontal axis in Fig. 1. We draw a spiral pattern as shown in Fig. 1b. For every k, this pattern is transformed by means of Eq. (12), which merely represents an enlargement (12a) and a rotation (12b) of the pattern. If all these transformed patterns are overlayed, the "best" position of the LSR is the point that all patterns have in common.

We approached this problem by computing a crude pattern from our solution by finding those positions where the surface density ϱ_s reaches a maximum in the radial direction. These positions were then transformed by Eq. (12) for every k, and the resulting patterns were overlayed on a Comtal Vision One image-processing system, using a different color for every pattern.

The method turned out to be unsuccessful, for reasons that can be easily understood. First, it was difficult to find a reliable set of l_k-values from the observations. One set we used was $\{-80°, -60°, -35°, -22°, 30°, 50°\}$. Here the inaccuracy is about 5°. Secondly, the method yielded about 10 candidates with this set. Thirdly, the corresponding model (l,v)-diagrams showed quite interesting features, but none of them looked very satisfactory. In many cases the expected bumps or peaks did not show up at all, despite the obvious presence of an arm at the tangential point. This indicates that the method of the tangential points is not likely to be useful for the determination of spiral arms from the observations. It clearly is not useful for the present purpose.

Because of these disappointing results, we continued with a second approach. In the above, local extrema in the tangential-point velocities are interpreted as indicators of spiral arms near the tangential points. Instead of extrema in the radial velocity for varying longitude, one may consider extrema in longitude for varying velocity. These "turning loops" clearly must be associated with spiral arms. At the extremum, the line of sight coincides with the line tangent to the spiral arm. In the previous method, it turned out that the arms in our model not always reach the envelope of the (l,v)-diagram. The identification of a turning loop (an extremum in longitude) involves structures that extend over larger portions of the (l,v)-diagram, and therefore seems more appropriate. One again can try to find a set of longitudes $\{l_k\}$ with $|l_k|<90°$ from the

observations, draw straight lines at these angles through one point on a transparancy and adjust this over Fig. 1 until every line is tangent to one of the spiral arms. The point at which all the lines intersect is the position of the LSR. The limitation of this method again is the irregular nature of the observed gas, which complicates the identifications of turning loops. One set of longitudes might be $\{-80°, -55°, -35°, -22°, 33°, 55°\}$, with an uncertainty of about 5°. A large number of positions for the LSR can be found that are reasonably consistent with the larger part of this set. There is a multiplicity that arises from the more or less self-similar character of a spiral arm. For a perfect, infinite two-armed logarithmic spiral, the present method would be inadequate. This pattern would look the same from all angles, for all radii at some fixed distance from the nearest spiral arm. For our gas-dynamical model, the method of lines tangent to spiral arms provides some information, but the uncertainty in the identification of turning loops, combined with the effects of multiplicity, makes is impossible to find an unique position for the LSR.

Fortunately, the observations contain some easily recognized features that can be used rather unambiguously to sort out a position for the LSR. The one of most importance to this work is the 3-kpc arm. It has an "expansion" of about 50 km s^{-1} at zero longitude, and occurs on our side of the GC (van Woerden et al., 1957; cf. Oort, 1977). To find the azimuth ϕ_{LSR}, we only have to make a plot of the radial velocity u_R (u_R is radial with respect to the GC) and to look for an arm having a positive velocity of about 50 km s^{-1}. Figure 2 shows u_R/c, the radial velocity plotted as a mach number. For a sound speed of about 10 km s^{-1}, we indeed can identify an arm with the correct "expansion". The arm is sketched in Fig. 3. For a bar with an axial ratio 0.7, we find a range of angles ϕ_{LSR} between 16° and 36° where the velocity u_R/c exceeds 4. For a weaker bar with an axial ratio 0.75 this range vanishes, leaving a highest value around 30° that is smaller than 4. For a stronger bar with an axial ratio 0.65, the range lies between 11° and 43°.

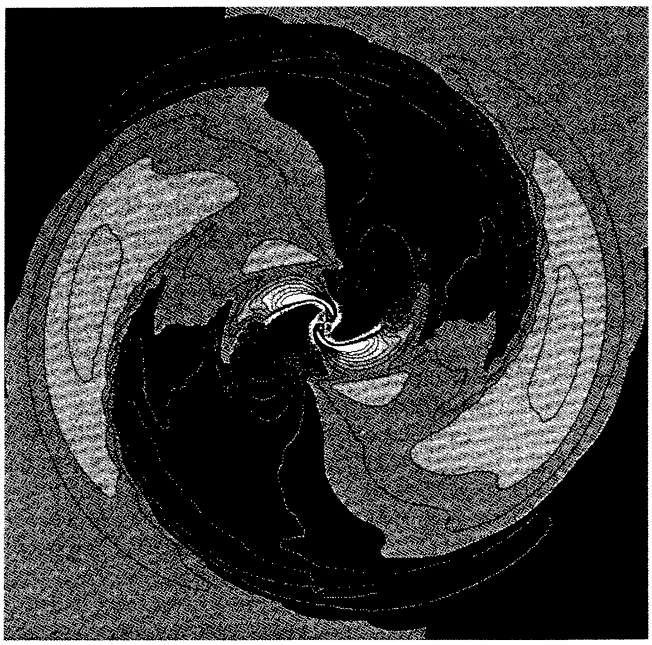

Fig. 2. The radial velocity with respect to the galactic centre scaled to the sound speed, u_R/c, for the model presented in Fig. 1. Contours are drawn at integer values of the mach number u_R/c from −7 to 7. The lighter shades corresponds to negative velocities, the darker to the positive

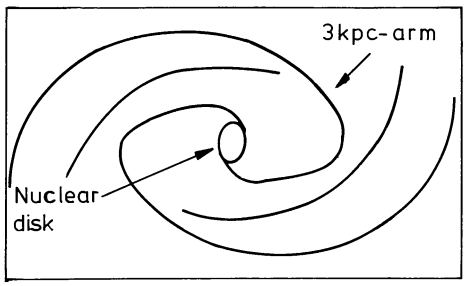

Fig. 3. Sketch indicating the nuclear ring and the 3-kpc arm

Our model 3-kpc arm lies in a region of "expansion". This expansion is due to the elliptical character of the streamlines. As can be seen from Fig. 2, there is a region within the central ring, where the "expansion" takes place in the second quadrant (defined by $90° < \phi < 180°$). Across the ILR the region of "expansion" gradually rotates to the first quadrant ($0° < \phi < 90°$), until, around the OLR, it again rotates to the second quadrant. In terms of elliptical streamlines, this implies that the streamline-ellipses have their long axis in the vertical direction within the ILR and beyond the OLR, and in the horizontal direction between these Lindblad Resonances. This behaviour has been described by Contopoulos (1980) while considering the shape of periodic orbits. It implies that it must be possible to construct a self-consistent bar all the way up to the OLR.

If Figs. 1 and 2 are compared, it turns out that the 3-kpc arm is formed by an arm of high density behind a shock, with a local radial velocity u_R smaller than that of the surrounding flow field. The systematic ellipsoidal character of the overall flow pattern provides sufficient "expansion" to compensate the dip in the radial velocity. Therefore, this feature still shows up as an "expanding arm" with respect to the GC.

The second feature to be considered is the "nuclear disk" (cf. Oort, 1977), the disk with the high velocities near the galactic centre. Figure 4 shows (l, v)-diagrams for the central part of our model between longitudes −15° and 15°, as seen from various angles ϕ_{LSR}, assuming a provisional distance $R_{LSR} = 10$ model units. At first sight, it seems that an azimuth around 90° would be best (compare Fig. 6). However, in that case the positive "forbidden" velocities for $l < 0°$ cannot be explained. For ϕ_{LSR} around 0°, we get a band of "forbidden" velocities on both sides of the GC. These velocities are less prominent in the observations at positive longitudes and negative velocities, but are certainly there (see, e.g., Burton and Liszt, 1983, Fig. 4g). The observed asymmetry is probably due to extensive absorption against the nuclear continuum emission sources.

If we combine our findings for the 3-kpc arm and the centre, we must conclude that ϕ_{LSR} lies on the lower side of the interval between 16° and 36°. We choose to fix ϕ_{LSR} at 20°.

The distance R_{LSR} to the galactic centre can now be found by trial and error. We have made a series of (l, v)-diagrams at $\phi_{LSR} = 20°$ for various R_{LSR}. Figure 5 shows the result for $R_{LSR} = 8.5$ and $\phi_{LSR} = 20°$, which we present as our "best" position of the LSR in our model. The main criterion for selecting the distance of 8.5 model units is the observed ridge at about −50 km s^{-1} between longitudes 90° and 140°. For the computation of the (l, v)-diagram, the disk has been cut off at 25 model units, which is just outside the outer ring. The average neutral hydrogen density $n_{HI,0} = 0.6$ cm^{-3}. The scales of our model become, through Eqs. (6) and (7): $r_0 = 1.18$ kpc and $u_0 = 310$ km s^{-1}, implying a sound speed $c = 10.9$ km s^{-1}.

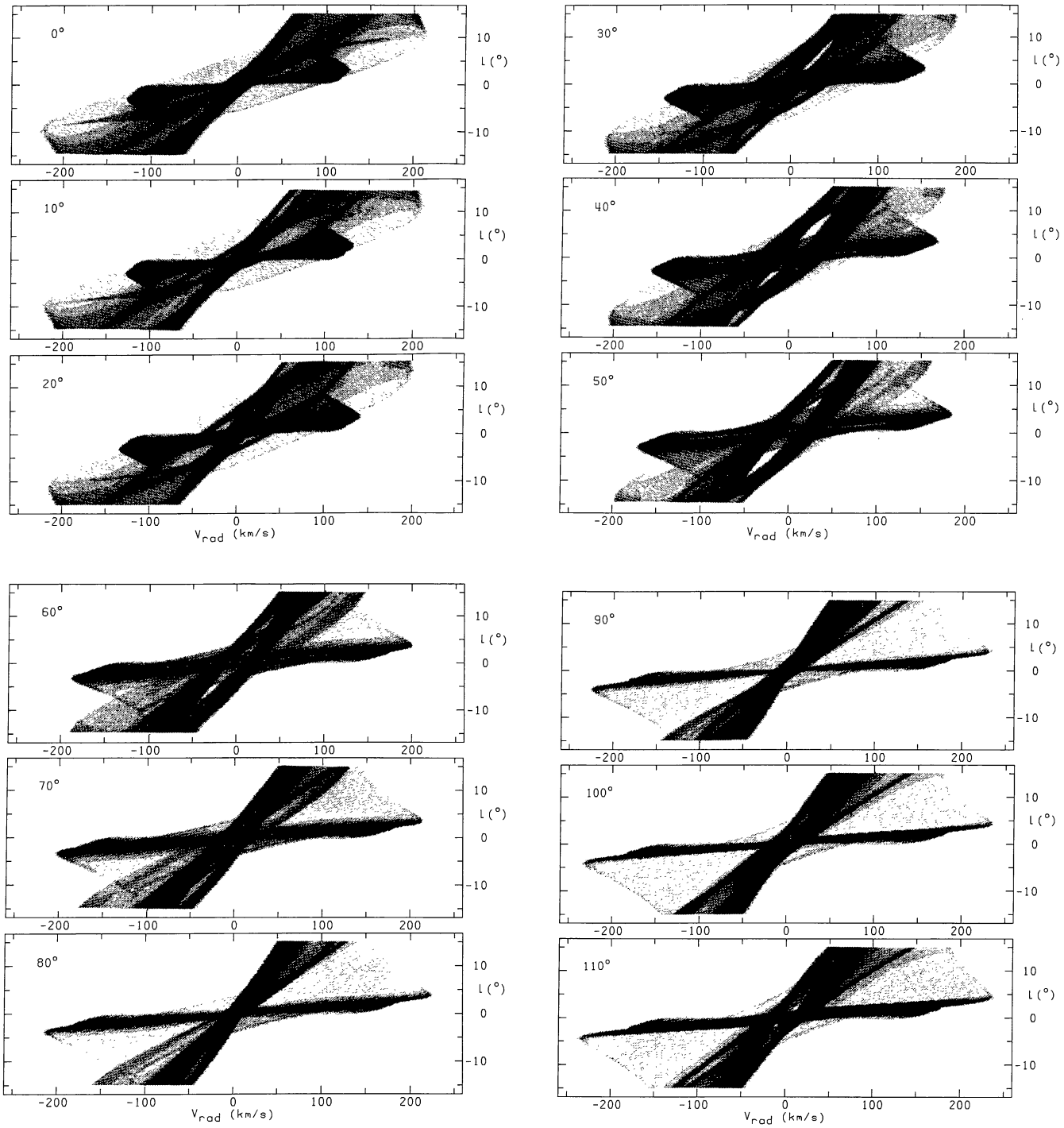

Fig. 4. (l, v)-diagrams for the central part of our model, at different values of ϕ_{LSR}. The assumed provisional distance R_{LSR} of the LSR to the centre is 10 model units

Figure 6 shows the observed (l, v)-distribution. The data are taken from the Leiden-Greenbank survey (Burton, 1985). The longitudes between 267° and 339° are taken from the Parkes survey by Kerr et al. (1981).

4. Discussion

Now that we have made a choice for the position of the LSR in our model, we can compare the model with the observations. An exact correspondence can not be expected with our crude guess of the galactic potential, but the model should at least give a qualitative explanation for a number of features in the observations. Before discussing this in some detail, we consider the influence of the density distribution and the velocity field on the model (l, v)-diagram.

Figure 7a shows the influence of the model velocity field. Here the surface density has been taken from the model, but the velocity field has been replaced by purely circular rotation, following the

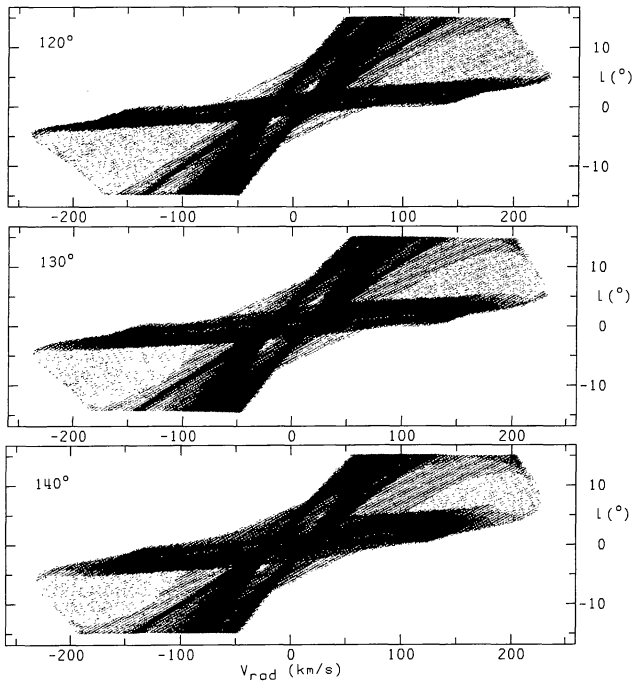

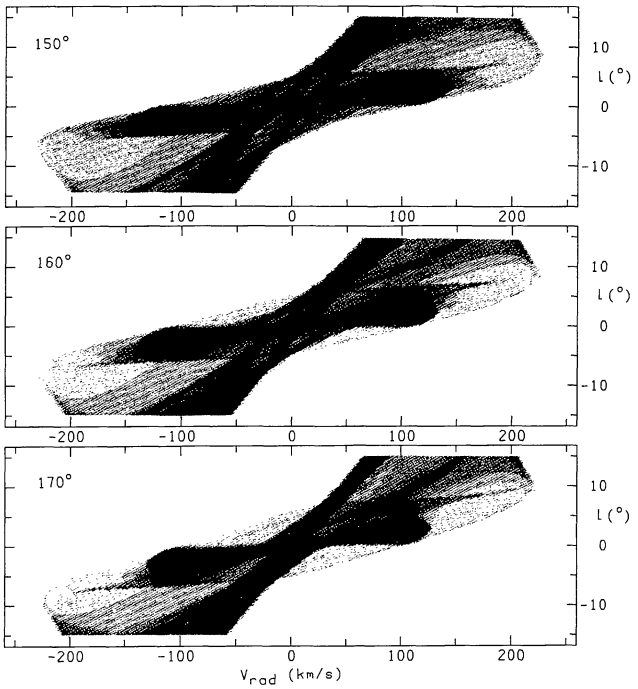

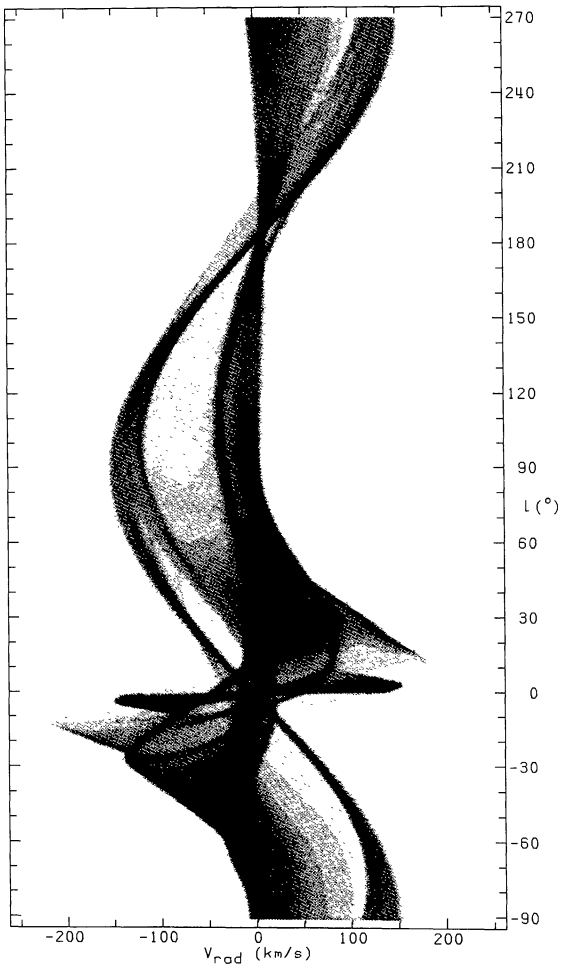

Fig. 5. Model (l, v)-diagram for $R_{LSR}=8.5$ and $\phi_{LSR}=20°$

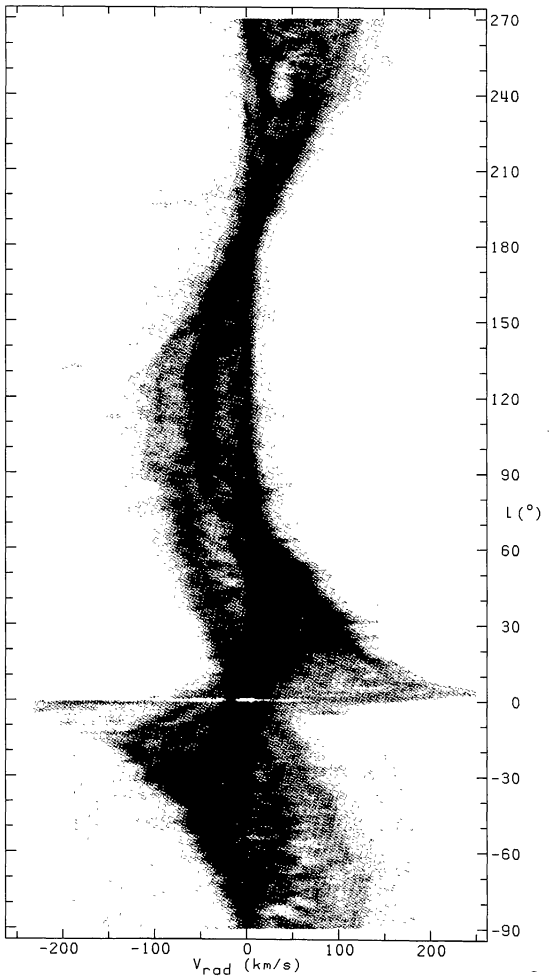

Fig. 6. A (l, v)-diagram based on observations of neutral hydrogen by Burton (1985) and Kerr et al. (1981)

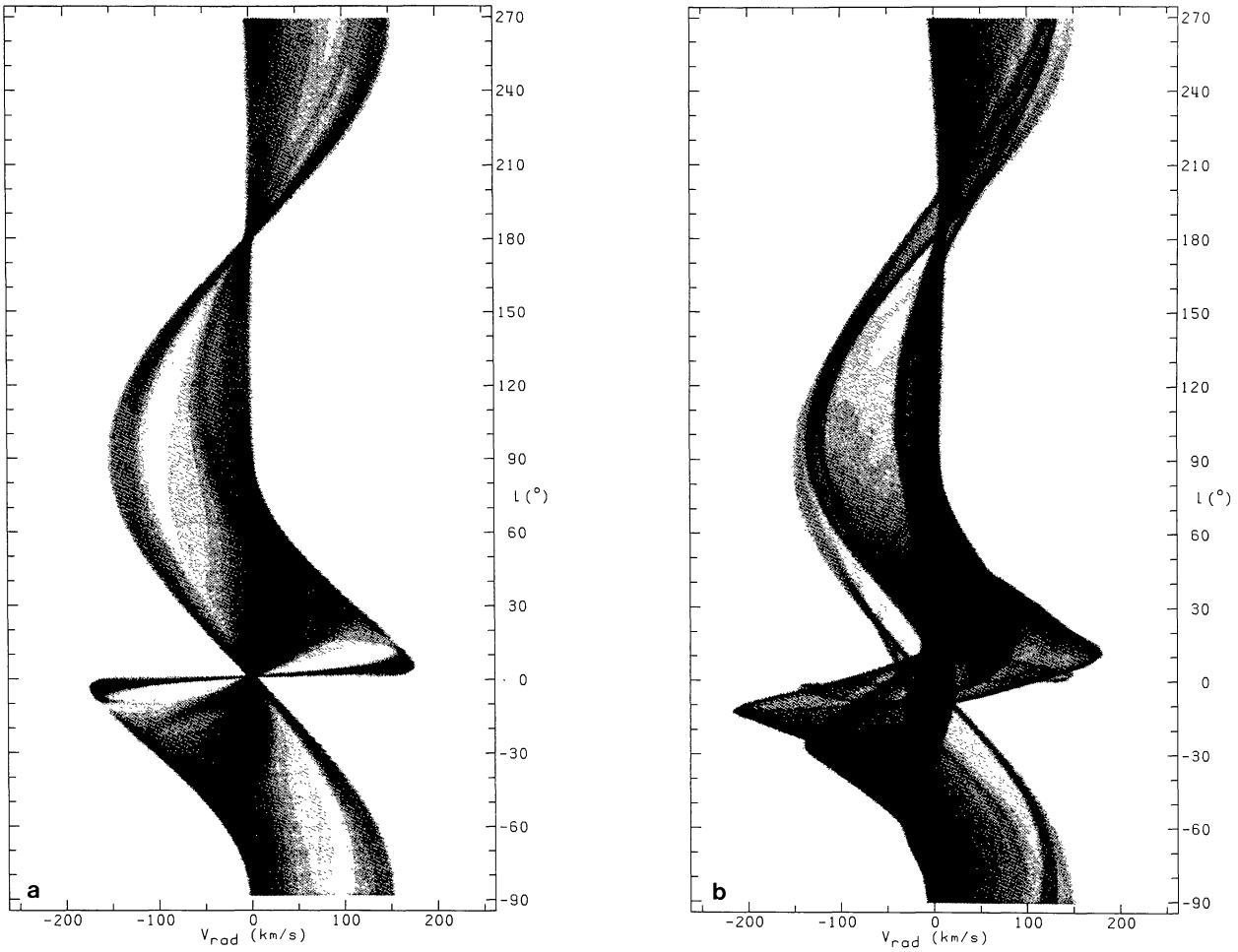

Fig. 7. a Model (l, v)-diagram similar to Fig. 5, but the velocity field has been replaced by axisymmetric rotation. Only the surface density is taken from the numerical quasi-steady state. **b** Model (l, v)-diagram similar to Fig. 6, but now the surface density is kept constant and the velocity is derived from the numerical solution

axisymmetric part of the potential. Most of the features have disappeared; others are only weakly present. Figure 7b shows a (l, v)-diagram with the proper velocity field, but now the surface density has been kept constant. The resulting (l, v)-diagram looks quite similar to the original one. We conclude that the features in the (l, v)-distribution are mainly determined by the *velocity field* of our solution. *Velocity crowding* is much more important than the occurrence of high-density arms. This confirms the conclusions by Burton (1971) and Liszt and Burton (1982). Any interpretation or modeling of the observed (l, v)-diagram that is carried out on the assumption of circular rotation and that tries to find a global pattern on the basis of high-density arms must yield incorrect results, if in fact velocity perturbations of amplitude more than a few km s^{-1} are present.

We continue with the discussion of several features in our model (l, v)-diagram as compared to the observations. Figure 8 shows where the various arms that are sketched in Fig. 1b, appear in the (l, v)-diagram. An arm is defined by a distinct density enhancement associated with a shock. We have included the offshoots of these arms where the shocks have disappeared but the density is still higher that that of the surrouding material. Some of these arms are discussed below. We will look for corresponding features in the observations.

As already mentioned in Sect. 3, the central ring has high-velocity wings that exceed the circular velocity corresponding to the axisymmetric part of the potential. Any mass model based on an interpretation of these high-velocity peaks in terms of circular motion is bound to overestimate the central mass in our Galaxy (a similar suggestion has been made by Burton and Liszt, 1978). Most mass models for our Galaxy, e.g., by Schmidt (1965), Oort (1977), Caldwell and Ostriker (1981), and Bahcall et al. (1982), incorporate a massive central component to account for the high-velocity peak near the centre. The smooth power law used in this paper is, because of its bar-like shape, capable of creating the high-velocity peaks without such a massive component. Recently, Sellwood (1985) has studied the gravitational stability of the model by Bahcall et al. (1982) by means of an N-body code, and showed that a bar forms if the massive central component is removed. In this way, we obtain a consistent picture on the basis of a mass model without a massive central component, like the one used here. An initially axisymmetric mass distribution with a gently rising rotation curve develops a bar that drives the spiral pattern.

The 3-kpc arm has already been discussed in Sect. 3, where we have used this feature to find the azimuth of the LSR. In our model it corresponds to the ILR-arm at the near side of the GC. It reaches an extremum of negative radial velocity at a longitude of about $-20°$ and then turns back towards the centre of the (l, v)-diagram. This is consistent with the observations. The counterpart of this arm on the far side of the GC has a somewhat different behaviour, due to the perspective. It has a positive velocity at $l=0°$ that is

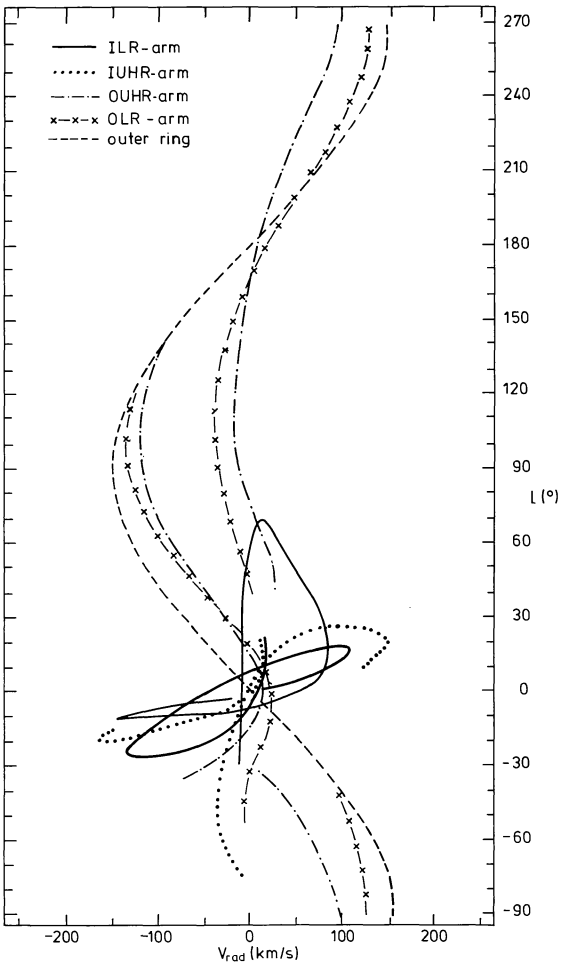

Fig. 8. Sketch of some features in the model (l, v)-diagram

higher (in absolute value) than that of the 3-kpc arm. However, for negative longitudes it turns very quickly to negative velocities, causing a distinct asymmetry in the (l, v)-diagram. At $l = -10°$, it appears as a thin line going to negative velocities at an almost constant longitude. For positive longitudes, this arm bends towards the envelope of the (l, v)-diagram at the positive velocities, until, just inside the LSR (cf. Fig. 1a, where the LSR is indicated by ⊙), it turns again to smaller longitudes and becomes practically indistinguishable. The part of this arm near zero longitude may be identified with the van der Kruit feature VII (1970) in the observations.

Between longitudes 10° and 20° the observations show the "connecting arm" (van der Kruit feature III, 1970; Cohen feature IIIa, 1975) at the positive velocity envelope. This "arm" is also found in the model (l, v)-diagram, as the effect of velocity crowding in the smooth part of our velocity field.

The model (l, v)-diagram does not show many distinct features between 30° and 80° at positive velocities. At about 30° there is an offshoot of the inner UHR-arm on the near side of the centre, but its radial velocity does not exceed that of the "connecting arm". Near about 55° a weak ridge reaches a maximum positive velocity. However, this maximum is not high enough to produce a bump in the envelope of the (l, v)-diagram. It is caused by a part of the outer UHR-arm that passes the anticentre just outside the LSR.

In the interval between $-80°$ and $-30°$ there is also not much distinct structure in our model (l, v)-diagram. A weak offshoot of the outer UHR-arm almost reaches the envelope of the (l, v)-diagram at negative velocities. A distinct ridge with a negative velocity comes all the way from the positive longitudes towards the negative, until it reaches an extremum of about $-40\,\mathrm{km\,s^{-1}}$ around $-50°$. Between $-60°$ and $-80°$ it causes a bump in the envelope and then gradually disappears. This ridge is due to the inner UHR-arm at the near side which has been mentioned above. A similar ridge is not clearly present in the observations.

At a longitude of about 40°, near zero velocity, the OLR-arm starts and sets off towards $-50\,\mathrm{km\,s^{-1}}$ as l increases. The correspondence with the observations is obvious, and for that reason this arm was used to determine the distance of the LSR to the centre in our model. The arm can be followed throughout the model (l, v)-diagram until, at about $-40°$ it reaches the outer ring. The other OLR-arm at the opposite side of the GC, can be followed from the outer ring at about 120° on the negative-velocity side of the model (l, v)-diagram. For decreasing l, its velocity increases more rapidly than that of the outer ring as its distance to the GC decreases, until, at about $-50°$ it vanishes. This arm and the outer ring can be identified with the double structure at negative velocities between 10° and 50° in the observations.

The anticentre is another region of interest. The observations show an inclined ridge that has zero velocity at about 185° rather than 180°. A similar behaviour can be found in our model: there is a crossing at longitude 185° of the ridge associated with the outer ring and the ridge associated with the local gas. This shift to a higher longitude is caused by the slight positive radial velocity of the gas just outside the radius of the LSR (cf. Fig. 2). Outside the OLR-arm, the radial velocity suddenly becomes negative. This gives rise to a wing of negative velocities around the anticentre, which is also present in the observations (see also: Burton and Moore, 1979, Fig. 3).

An obvious shortcoming of our model is the magnitude of the velocities at large radii. This may be amended by adopting a bar that is weaker around the OLR. This will cause the shock of the OLR-arm to end at a smaller radius. As the outer ring is created by material that is pushed outwards by dissipation in the shocks outside CR, this ring will occur at a smaller radius, thus reducing the apparent velocity in the (l, v)-diagram. On the other hand, if the bar is cut off at CR, our model does not have shocks outside CR. In that case, the OLR-arm is not present [apart from a very slight density enhancement that does not show up in the (l, v)-diagram] and the $-50\,\mathrm{km\,s^{-1}}$ ridge between 90° and 140° can not be explained. Clearly, we need a function $c_2(R)$ in Eq. (1) that is somewhere between a bar extending to the OLR and one ending at CR.

An entirely different amendment for the high velocities around 90° in the model can be obtained if the $-50\,\mathrm{km\,s^{-1}}$ ridge between 90° and 140° is represented by the outer ring rather than the OLR-arm. This requires a larger value for R_{LSR}. The larger distance to the GC causes the longitude of $-20°$, where the 3-kpc arm turns, to move towards the centre. This can be compensated by increasing the azimuth ϕ_{LSR}, thus enlarging the longitudinal extent of the 3-kpc arm. At the same time, a stronger bar is required to maintain the correct "expansion". In addition, the longitudinal extent of the 3-kpc arm may be enlarged by changing the power p. This power is related to the radial scaling of the spiral pattern. A value closer to -2 brings the locations of the ILR, IUHR, OUHR, and OLR closer to CR, thus reducing the pitch angle of the spiral arms, enlarging the central region of the model, and shrinking the region around CR.

Figure 9 illustrates the above effects and gives an impression of the room to manoeuvre with the present class of models. We have

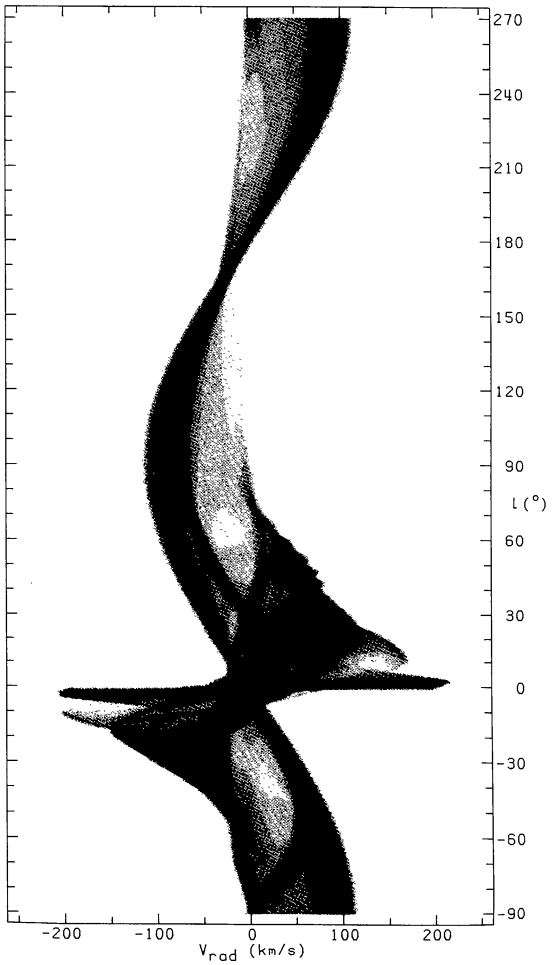

Fig. 9. Model (l, v)-diagram for a potential with a power $p=-1.95$ and an axial ratio of the bar $b/a=0.65$. The LSR is now at $R_{\rm LSR}=15$ and $\phi_{\rm LSR}=40°$

changed just about all relevant parameters: the power of the potential $p=-1.95$ and the axial ratio of the bar $b/a=0.65$. The pattern speed $\omega=0.083891$, bringing CR at the same radius as in the previous model. Oualitatively, the quasi-steady state is very similar to the one presented in Fig. 1, but the spiral arms have a smaller pitch angle and are slighly more concentrated around CR. The position of the LSR has been chosen just outside the OLR-arm: $R_{\rm LSR}=15$ and $\phi_{\rm LSR}=40°$. The present value of p effectively increases the central velocities of the "nuclear disk". For the tangential velocity $u_{\phi,\rm LSR}$ of the LSR we have used the local value of the gas instead of the one prescribed by Eq. (7). The latter is considerably smaller than the first (about 22 km s^{-1}); using the latter will result in the absence of gas with zero velocity $v_{\rm rad}$ in the region between 90° and 270°. The radial velocity $u_{R,\rm LSR}$ is set to zero, as before. The jagged structure in the (l, v)-diagram around 50°, where the nearby OLR-arm turns, is caused by the computational grid of our quasi-steady solution. It should be emphasized that most of the differences between Figs. 5 and 9 arise from the change in position of the LSR. Furthermore, this last choice of parameters and of a position for the LSR is *not* proposed as a serious candidate for a global galactic model. The remainder of this paper refers to the first choice.

An independent estimate of the position of the LSR has been given by Mulder (1983) on the basis of a simple model for the warp of our Galaxy. The gravitational potential in that paper is more or less the same as the one used here. A family of stable periodic orbits at the vertical 1 : 1 resonance is proposed as a model for the warp. The orbits are almost circular and tilted with respect to the equatorial plane. If these orbits describe the warp correctly, the line of nodes of the warp should coincide with the short axis of the bar. The distance $R_{\rm LSR}$ was found to be 11.6 model units, which, in view of the uncertainties in that and in this paper, is not in contradiction with the present value. However, as the line of nodes is at $-10°$ from the sun, as seen from the galactic centre (Henderson et al., 1982), we must have either $\phi_{\rm LSR}=80°$ or 100°. This indicates that the simple warp model is too simple. On the other hand, if a stable steady or quasi-steady pattern at the same vertical 1 : 1 resonance, but rotated by 90°, could be obtained, this would be practically consistent with the present work. It may be worthwile to investigate the effect of a pressure-term on the motions around this resonance.

5. Concluding remarks

Our initial model is successful in explaining a number of distinct features in the observed neutral hydrogen longitude-velocity distribution. The position of the LSR in the model could be found by concentrating on the nuclear disk, the 3-kpc arm, and the OLR-arm between longitudes 90° and 140° at -50 km s^{-1}. We found a distance $R_{\rm LSR}$ of the Local Standard of Rest to the Galactic centre of 8.5 model units, which is in the region of co-rotation. The azimuth $\phi_{\rm LSR}$ is 20°, measured counterclockwise with respect to the long axis of the bar. There is not much freedom to choose a different position, at least not more than by about ± 2 model units of length and $\pm 20°$. The axial ratio of the bar should be 0.7 at most in the region within co-rotation. A weaker bar (0.75) cannot give a high enough apparent "expansion" for the 3-kpc arm.

The bar-like perturbation to our simple power-law potential is sufficient to provide large non-circular motions. These can explain the high-velocity wings near the centre, the "expansion" of the 3-kpc arm, and the "forbidden" velocities in the centre and anticentre. The rotation curve that corresponds to the axisymmetric part of the potential is gently rising. No massive central component is required to account for the high-velocity peaks near the centre.

The model (l, v)-diagram is mainly determined by the velocity field of the model. If the model is correct, then the interpretation of the observed (l, v)-distribution in terms of high-density arms and almost circular motion must yield incorrect results.

Our initial guess of the Galactic potential yields surprisingly good results. Therefore, a gas-dynamical approach towards the problem of the large-scale structure in our Galaxy seems to be a promising one.

Acknowledgements. The authors are indebted to P. te Lintel Hekkert for his assistance in the preparation of Fig. 6, and to Prof. W.B. Burton for helpful discussions and comments on the manuscript.

References

Bahcall, J.N., Schmidt, M., Soneira, R.M.: 1982, *Astrophys. J.* **258**, L23

Burstein, D., Rubin, V.C., Thonnard, N., Ford, W.K.: 1982, *Astrophys. J.* **253**, 70

Burton, W.B.: 1971, *Astron. Astrophys.* **10**, 76
Burton, W.B., Liszt, H.S.: 1978, *Astrophys. J.* **225**, 815
Burton, W.B., Moore, R.L.: 1979, *Astron. J.* **84**, 189
Burton, W.B., Liszt, H.S.: 1983, *Astron. Astrophys. Suppl. Ser.* **52**, 63
Burton, W.B.: 1985, *Astron. Astrophys. Suppl. Ser.* **62**, 285
Caldwell, J.A.R., Ostriker, J.P.: 1981, *Astrophys. J.* **251**, 61
Cohen, R.J.: 1975, *Monthly Notices Roy. Astron. Soc.* **171**, 659
Contopoulos, G.: 1980, *Astron. Astrophys.* **81**, 198
Henderson, A.P., Jackson, P.D., Kerr, F.J.: 1982, *Astrophys. J.* **263**, 116
Isaacman, R.B.: 1981, *Astron. Astrophys.* **95**, 46
Kerr, F.J.: 1967, in *Radio Astronomy and the Galactic System*, IAU *Symp.* **31**, ed. H. van Woerden, Academic Press, New York
Kerr, F.J., Bowers, P.F., Henderson, A.P.: 1981, *Astron. Astrophys. Suppl. Ser.* **44**, 63
Kulkarni, S.R., Blitz, L., Heiles, C.: 1982, *Astrophys. J.* **259**, L63
Liszt, H.S., Burton, W.B.: 1982, *Astrophys. J.* **243**, 778
Liszt, H.S.: 1985, in *The Milky Way Galaxy*, IAU *Symp.* **106**, eds. H. van Woerden, R.J. Allen, W.B. Burton, Reidel, Dordrecht, pp. 283–300
Mulder, W.A.: 1983, *Astron. Astrophys.* **121**, 91
Mulder, W.A., Hooimeyer, J.R.A.: 1984, *Astron. Astrophys.* **134**, 158 (Paper I)
Mulder, W.A.: 1986, *Astron. Astrophys.* **156**, 354 (Paper II)
Oort, J.H.: 1977, *Ann. Rev. Astron. Astrophys.* **15**, 295
Peters, W.L.: 1975, *Astrophys. J.* **195**, 617
Roberts, W.W.: 1971, *Bull. Amer. Astron. Soc.* **3**, 369
Rubin, V.C., Ford, W.K., Thonnard, N.: 1982, *Astrophys. J.* **261**, 439
Sanders, R.H., Lowinger, T.: 1972, *Astron. J.* **77**, 292
Schmidt, M.: 1965, in *Stars and Stellar System: Vol. 5, Galactic Structure*, eds. A. Blaauw, M. Schmidt, Univ. of Chicago Press, Chicago, pp. 513–530
Sellwood, J.A.: 1985 (preprint)
Shu, F.H., Milione, V., Gebel, W., Yuan, C., Goldsmith, D.W., Roberts, W.W.: 1972, *Astrophys. J.* **173**, 557
Simonson, S.C.: 1976, *Astron. Astrophys.* **46**, 261
Spitzer, L.: 1978, *Physical Processes in the Interstellar Medium*, Wiley, New York
van Albada, G.D.: 1985, in *The Milky Way Galaxy*, IAU *Symp.* **106**, eds. H. van Woerden, R.J. Allen, W.B. Burton, Reidel, Dordrecht, pp. 547–549
van der Kruit, P.C.: 1970, *Astron. Astrophys.* **4**, 462
van Woerden, H., Rougoor, G.W., Oort, J.H.: 1957, *Comptes Rendus* **244**, 1691
Yuan, C.: 1969, *Astrophys. J.* **158**, 871
Yuan, C.: 1984, *Astrophys. J.* **281**, 600